THE JOURNAL OF PHYSICAL CHEMISTRY B
A JOURNAL OF THE AMERICAN CHEMICAL SOCIETY
pubs.acs.org/JPCB

Article

Molecular Modeling and Simulation of Polymer Nanocomposites with Nanorod Fillers

Published as part of The Journal of Physical Chemistry virtual special issue "Carol K. Hall Festschrift".

Shizhao Lu,[#] Zijie Wu,[#] and Arthi Jayaraman*

Cite This: *J. Phys. Chem. B* 2021, 125, 2435−2449

Read Online

ACCESS | Metrics & More | Article Recommendations | Supporting Information

ABSTRACT: We present a coarse-grained (CG) molecular dynamics (MD) simulation study of polymer nanocomposites (PNCs) containing nanorods with homogeneous and patchy surface chemistry/functionalization, modeled with isotropic and directional nanorod−nanorod attraction, respectively. We show how the PNC morphology is impacted by the nanorod design (i.e., aspect ratio, homogeneous or patchy surface chemistry/functionalization) for nanorods with a diameter equal to the Kuhn length of the polymer in the matrix. For PNCs with 10 vol % nanorods that have an aspect ratio ≤5, we observe percolated morphology with directional nanorod−nanorod attraction and phase-separated (i.e., nanorod aggregation) morphology with isotropic nanorod−nanorod attraction. In contrast, for nanorods with higher aspect ratios, both types of attractions result in aggregated nanorods morphology due to the dominance of entropic driving forces that cause long nanorods to form orientationally ordered aggregates. For most PNCs with isotropic or directional nanorod−nanorod attractions, the average matrix polymer conformation is not perturbed by the inclusion of up to 20 vol % nanorods. The polymer chains in contact with nanorods (i.e., interfacial chains) are on average extended and statistically different from the conformations the matrix chains adopt in the pure melt state (with no nanorods); in contrast, the polymer chains far from nanorods (i.e., bulk chains) adopt the same conformations as the matrix chains adopt in the pure melt state. We also study the effect of other parameters, such as attraction strength, nanorod volume fraction, and matrix chain length, for PNCs with isotropic or directional nanorod−nanorod attractions. Collectively, our results provide valuable design rules to achieve specific PNC morphologies (i.e., dispersed, aggregated, percolated, and orientationally aligned nanorods) for various potential applications.

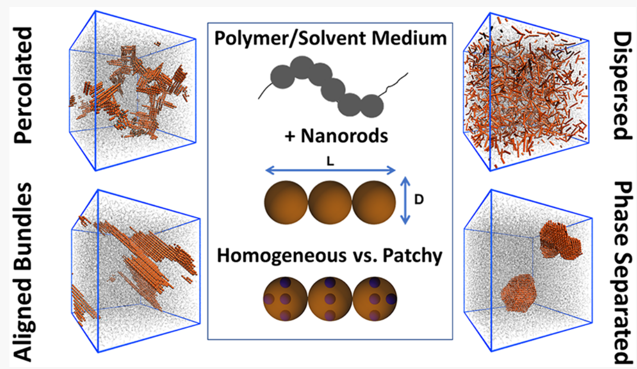

I. INTRODUCTION

Polymer nanocomposites (PNCs) are materials comprised of polymers and nanoscale fillers that exhibit improved macroscopic properties compared to the filler-free polymers. These macroscopic properties are strongly dependent on the filler size, shape (e.g., spherical nanoparticles, nanorods, nanosheets, etc.), chemistry, and their microscopic spatial arrangement (e.g., dispersed, aggregated, strings, percolated states).[1−9] Specifically, PNCs with nanorods or nanowires as fillers exhibit unique enhancement in mechanical (e.g., higher elastic modulus,[10,11] lower rheological percolation threshold[12]), electrical (e.g., lower electrical percolation threshold,[12,13] higher ionic conductivity[14]), thermal (e.g., higher thermal conductivity[15,16]), and optical (e.g., more conducive to polarization[17−19]) properties compared to PNCs with spherical nanoparticles, owing to the morphologies that are more readily accessible to the anisotropic one-dimensional nanorods. For example, percolated networks of carbon nanotubes or nanowires in PNCs have low concentration thresholds for conductivity.[2,8] In another example, PNCs with orientationally aligned assembly of silica carbide nanorods in epoxy resin have been demonstrated to have higher thermal conductivity compared to PNCs with randomly oriented nanorods.[16] As advances in nanorod synthesis and design allow for new physical and chemical nanorod features,[20,21] there is a growing need for connecting PNC morphologies to these physical and chemical design features of the nanorods as this connection is key to tailoring the morphology of the PNC toward desired macroscopic properties.

Molecular simulations are powerful tools to microscopically probe and predict PNC morphologies for various PNC design parameters. Past simulation studies have focused on specific

Received: January 5, 2021
Revised: February 13, 2021
Published: March 1, 2021

https://dx.doi.org/10.1021/acs.jpcb.1c00097
J. Phys. Chem. B 2021, 125, 2435−2449

rod-shaped filler chemistries such as carbon nanotubes,[22] cellulose nanocrystals,[23] or polymer grafted nanorods[24−26] as well as PNCs with bare nanorods[27−29] to understand universal phase behavior. For example, using Monte Carlo (MC) and coarse-grained molecular dynamics (CGMD) simulations, Toepperwein et al. have found that in PNCs with attractive matrix−nanorod interaction, long nanorods (aspect ratio of 16) aggregate in bundles and exhibit high short-range orientational alignment compared to short nanorods (aspect ratio of 8) that are dispersed at the same volume fraction of 0.10.[27,28] Surve et al. have studied the phase behavior of nanorods in polymer solutions with attractive nanorod-polymer interaction using self-consistent-field theory (SCFT), and have found that the width of the miscibility window in terms of nanorod volume fraction decreases with increasing nanorod aspect ratio and nanorod diameter. They have also found that either repulsive or strong attractive matrix−nanorod interaction is good for miscibility of nanorods.[30] Along the same lines, Sankar and Tripathy have used the Polymer Reference Interaction Site Model (PRISM) theory to find that the miscibility window becomes smaller with increasing nanorod aspect ratio and plateaus above a certain aspect ratio (∼10).[31] They have also observed that the miscibility window narrows with increasing nanorod−nanorod attraction as the effective matrix−nanorod interaction becomes more unfavorable, and the miscibility window exhibits a nonmonotonic trend with increasing nanorod diameter.

Another critical question in many of the PNC-focused simulations and experiments is how the matrix polymer conformation changes as a function of the nanofillers and the filler volume fraction.[32] In PNCs with *spherical* nanoparticles, several studies have shown that when the matrix−nanoparticle interaction is repulsive, the matrix chain conformations on average are not perturbed.[33−37] Contrary to these studies, Robbes et al. have shown that repulsive interaction between Fe_2O_3 nanoparticle and polystyrene matrix led to an expansion in the matrix chain conformation regardless of the state of nanoparticle dispersion.[38] When the matrix−nanoparticle interaction is favorable, matrix chains have been found, in both experiments and simulations, to either expand,[39−43] remain unperturbed[33,44,45] or contract.[46,47] Several factors have been shown to affect matrix chain conformations, including the following: ratio of characteristic length scales of matrix and nanoparticle, i.e., radius of gyration of polymer chain vs nanoparticle radius,[35,41,43] attractive/repulsive matrix−nanoparticle interaction,[33,36] strength of matrix−nanoparticle attraction,[48−50] nanoparticle mobility,[51,52] interparticle distance,[42,43,48,50] and nanoparticle state of dispersion.[38]

Moving from spherical nanoparticles to one-dimensional nanorods/nanotubes, Karatrantos et al. have found that in PNCs comprised of single walled carbon nanotubes (SWCNTs) with matrix chain radius of gyration, R_g, smaller than the nanorod radius, R_P, there is no change in matrix chain R_g at low filler volume fraction (=0.008).[22] A follow-up experimental study of PNCs with multiwalled carbon nanotubes (MWCNTs) and SWCNTs where the polymer matrix R_g was commensurate with the MWCNT radius but larger than the SWCNT radius has confirmed that polymer matrix conformation is not perturbed at low volume fraction of nanofiller (<0.02).[53] At a higher volume fraction (>0.02), they observed expansion of matrix chains in SWCNT nanocomposites. They observed no change in matrix chain conformations in MWCNT nanocomposites regardless of volume fraction. This difference in the response of matrix chain conformations to changing volume fraction of nanotubes between PNCs with SWCNT and MWCNT is attributed to the size of the two nanotubes. Another study from Toepperwein et al. reported up to 10% change in the average mean-squared end-to-end distance $\langle R_{ee}^2\rangle$ of matrix chains with the inclusion of nanorods at volume fraction of 0.05.[27]

The above examples demonstrate the complexity of the effect of fillers on the matrix chain conformation. To further complicate this, studies have suggested that it may be important to separately observe the behavior of interfacial chains (i.e., matrix chains that are in contact with nanoparticles),[33,54−57] and bulk chains (matrix chains that are not in contact with any of the nanoparticles). Starr et al. have shown that interfacial chains extend and flatten near the nanoparticle surface.[33] Huang et al. have found significant decrease in the R_g of interfacial chains in PNCs with strongly attractive matrix−nanoparticle system when the R_g is comparable to the nanoparticle radius.[58] To the best of our knowledge, none of the studies on nanorod/nanotube containing PNCs have separately analyzed the interfacial and bulk chain conformations. It is worth noting the difficulty in experimentally distinguishing interfacial chains as the signal is low due to the small fraction of interfacial chains.[34] As a result, the conformations of matrix chains reported experimentally are ensemble averages of all the matrix chains with little knowledge of the individual contributions of the interfacial and bulk chains in the matrix population. Additional effort from both the experimental side and the computational side is needed to investigate the impact of nanorods separately on the conformations of interfacial chains and bulk chains.

Lastly, we note that the computational studies presented above for PNCs with nanorods are aimed at nanorods/nanotubes with homogeneous surface chemistry, usually modeled by isotropic interactions between nanorods and/or between nanorod and matrix. To the best of our knowledge, no simulation studies have focused on nanorods with patchy/heterogeneous surface chemistry. Nanorods with heterogeneous or patchy surfaces have been synthesized via grafting[59] or functionalization[60] selectively on certain portions of the surface or via heterogeneity in the biological building blocks (e.g., peptides) that assemble to form the nanorods/nanowires.[61] It would be useful to understand how the above results highlighting universal or chemically specific trends in PNC morphologies for isotropically interacting, homogeneous nanorods change for PNC morphologies with directionally interacting, heterogeneous/patchy nanorods. The work presented in this paper addresses the need for a systematic and generic study comparing PNCs with homogeneous nanorods to PNCs with patchy nanorods as well as the need for distinguishing the effect of these nanorods' presence on interfacial and bulk matrix conformations. We will use the traditional approach of isotropic attractions between nanorods to model homogeneous surface chemistry and use a CG model of patchy nanorods that contain sites enabling directional attractions with sites on another nanorod surface.

The paper is organized as follows. In section II, we describe the PNC model, our simulation protocols, the parameter space we explored, and the analysis methods. In section III, we present and discuss the simulation results. In section IV, we conclude with a discussion on several design rules based on key results in this work.

https://dx.doi.org/10.1021/acs.jpcb.1c00097
J. Phys. Chem. B 2021, 125, 2435−2449

II. METHODS

II.A. Model. To represent the PNCs with nanorods interacting via *isotropic* repulsion or attraction, we use the "isotropic model". To represent the PNCs with nanorods interacting via *directional* attractions we use the "directional model". These two models are described next.

In the isotropic coarse-grained model, as shown in Figure 1a, the generic matrix polymer chains are represented with a bead–spring[62] model with each CG matrix bead of diameter $1d$ representing a Kuhn segment of the polymer. Each nanorod is modeled as a rigid body of connected nonoverlapping spheres. Choosing this physical representation of the nanorod over a smooth spherocylinder[63,64] or overlapping beads model[64] could bring a qualitative change to our simulation results, in particular, the entropic driving forces. However, we intentionally choose the rigid body of connected non-overlapping beads to model the nanorod over the smooth spherocylinder representation[63] for two reasons: (1) to facilitate a fair comparison to the directionally interacting nanorod model described next and (2) to enable future studies on effects of nanorod semiflexibility modeled by angle potentials imposed on consecutive nanorod beads. The diameter of the nanorod, D, is set to $1d$, focusing this study on modeling nanorods with diameter equal to the size of a Kuhn length of the matrix polymer. The length of the nanorod is equal to the integer number of D-sized nanorod beads to give an end-to-end length L (also in units of d). For example, an $L = 3d$ nanorod is a rigid body of three connected nonoverlapping beads each of diameter $1d$.

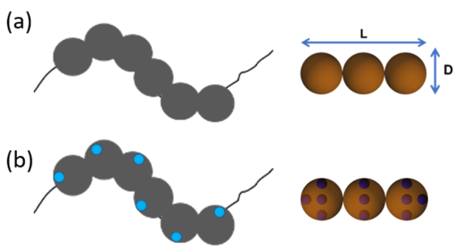

Figure 1. Schematic of the CG model for the (a) matrix chains and nanorods in PNCs with isotropic nanorod–nanorod attraction, and (b) matrix chains and nanorods in PNCs with directional nanorod–nanorod attraction. Embedded directional interaction sites are shown as cyan spheres in the gray polymer chain and darker spheres in the brown nanorod.

In the directional coarse-grained model, we embed additional directional interaction sites within each matrix bead and nanorod bead, as shown in Figure 1b. This directional interaction model is based on previous CG models used by Jayaraman and co-workers to study a variety of synthetic and biologically relevant polymers with directional interactions[65−74] as well as previous patchy particle models (see references to these in this viewpoint[75]). In this directional interaction model, each directional interacting site is a sphere of diameter $0.25d$ placed $0.37d$ from the center of its parent matrix bead of diameter $1d$ or nanorod bead of diameter D. The directional interaction site (cyan and dark blue sites in Figure 1b) is embedded within the parent matrix/nanorod bead. The net effect of the size and placement of these directional interaction sites is that (a) the interaction captured between two such sites is directional, as one would see in hydrogen bonding,[76] $\pi - \pi$ stacking,[77] and organometallic connections,[78] and (b) the excluded volume of the parent matrix or nanorod bead is not altered by the presence of these directional interaction sites. For the matrix polymers, one directional interaction site is placed on each matrix polymer CG bead. For the nanorods, the central (not end) nanorod beads have four equidistant sites each, and the two end beads each have one additional site (total five directional interaction sites per end bead). Even though we focus solely on attraction between nanorods in this study and always keep matrix–nanorod interaction purely repulsive, the installation of interaction sites on matrix beads facilitates future studies with matrix–nanorod attraction. Each nanorod and all its directional interaction sites are treated as a rigid body to reduce computational intensity without loss of realism.[79] In the matrix polymer, the distance between the site and the parent matrix bead is fixed, and together, the parent matrix bead and its directional interaction site are treated as a rigid body; this rigid body is connected to one or two adjacent matrix polymer CG bead(s) and their directional interaction site(s) the same way as in the isotropic model, via a harmonic spring with force constant of $50\frac{\epsilon}{d^2}$ where ϵ and d are reduced units of energy and length, respectively.

The isotropic nanorod–nanorod attraction is modeled using a 12–6 Lennard-Jones[80] (LJ) potential,

$$U_{LJ}(r) = \begin{cases} 4\epsilon_{LJ}\left[\left(\frac{\sigma_{LJ}}{r}\right)^{12} - \left(\frac{\sigma_{LJ}}{r}\right)^{6}\right], & r \leq r_{cut} \\ 0, & r > r_{cut} \end{cases} \tag{1}$$

with $\sigma_{LJ} = 1d$, $r_{cut} = 2.5d$, and ϵ_{LJ} equal to ϵ_{iso}, the strength of interaction that is varied in this study. The directional nanorod–nanorod attraction is captured by the interaction between directional interaction sites on different CG nanorod beads modeled using an LJ potential (as eq 1) with $\sigma_{LJ} = 0.25d$, $r_{cut} = 0.5d$ ($2\sigma_{LJ}$) and ϵ_{LJ} equal to ϵ_{dir}. Attractions between sites on the same nanorod are ignored as each nanorod is treated as a rigid body.

In this paper, we focus on PNCs in which the dominant interaction is the attraction between the nanorods. As such, all other pairwise interactions (matrix–matrix, matrix–nanorod, and nanorod–nanorod in directional model, directional interaction sites on matrix–directional interaction sites on nanorod, and directional interaction sites–other beads) are modeled with a purely repulsive, Weeks–Chandler–Andersen[81] (WCA) potential, as shown in eq 2, in both isotropic and directional models, with $\epsilon_{WCA} = 1kT$ and $\sigma_{WCA} = (\sigma_i + \sigma_j)/2$, where σ_i and σ_j are diameters of the two nonbonded beads.

$$U_{WCA}(r) = \begin{cases} 4\epsilon_{WCA}\left[\left(\frac{\sigma_{WCA}}{r}\right)^{12} - \left(\frac{\sigma_{WCA}}{r}\right)^{6}\right] + \epsilon_{WCA}, & r \leq 2^{1/6}\sigma_{WCA} \\ 0, & r > 2^{1/6}\sigma_{WCA} \end{cases} \tag{2}$$

II.B. Molecular Dynamics (MD) Simulation Protocol. We run molecular dynamics (MD) simulations in the *NVT* ensemble at reduced temperature $T^* = 1$ using the LAMMPS[82] package. The initial configuration is prepared by randomly placing both nanorods and fully extended matrix chains (i.e., rod-like configuration) in a large simulation box of size $150d \times 150d \times 150d$ with no overlap of any two CG beads. With all pairwise interactions set to repulsive only, the matrix chains are relaxed and mixed with the nanorods over 10 million time steps, where one time step is equal to 0.0005τ with τ being the reduced unit of time. Then, the large simulation box is gradually reduced in size over another 15 million time steps to achieve a final volume fraction, $\eta = \frac{\text{volume of all matrix CG beads and nanorod CG beads}}{\text{volume of the simulation box}} = 0.35$. From this point onward, the pairwise attractive interaction strengths are gradually increased to the desired values using a simulated annealing schedule that has been optimized to avoid kinetically trapped states in the PNCs. After achieving the desired attraction strength in both the isotropic and directionally interacting PNCs and equilibrating the system, we run the "production" part of the simulation for collection of uncorrelated configurations. The details (e.g., number of stages, time steps per stage) of the simulated annealing and production stage of the simulation used for isotropic or directional model PNCs are presented in the Supporting Information, Section SB. We collect five uncorrelated configurations from each of the three simulation trials and report the mean and standard deviation based on the total 15 uncorrelated configurations sampled for each PNC.

II.C. Analysis Methods. The configurations collected during the production stage of the MD simulations are used to quantify the morphology within the PNCs. We broadly categorize the nanorods structure to be in a dispersed state or in an aggregated state, which could be a phase-separated large cluster or many finite-sized clusters or a percolated state.

To quantify the spatial arrangement of the nanorods and matrix chains, we calculate intermolecular pair correlation functions, $g(r)$, between nanorod−nanorod and nanorod-matrix using

$$g_{pq}(r) = \frac{1}{4\pi r^2 N_p \rho_q} \sum_{i=1}^{N_p} \sum_{j=1}^{N_q} \delta(r - |\boldsymbol{R}_{p,i} - \boldsymbol{R}_{q,j}|) \tag{3}$$

where p, q are types of CG beads (matrix bead or nanorod bead), N_p is the number of CG beads of type p, ρ_q is the number density of q, and $R_{p,i}$ is the coordinate of the ith CG bead of type p. As we are interested in intermolecular pair correlation, if CG beads i and j are in the same matrix or same nanorod, they are excluded from the calculation.

To quantify the orientational order of nanorods in the PNC, we calculate the average orientational order parameter for each distance r, $\langle S_2(r)\rangle$.

$$\langle S_2(r)\rangle = \frac{\sum_{i=1}^{N_r}\sum_{j=i+1}^{N_r} \mathbf{1}_{r_{ij}\le r} P_2}{\sum_{i=1}^{N_r}\sum_{j=i+1}^{N_r} \mathbf{1}_{r_{ij}\le r}},$$
$$\text{where } P_2 = (3\cos^2\alpha_{ij} - 1)/2 \tag{4}$$

where i, j refer to two different nanorods in the simulation box, N_r is the total number of nanorods in the system, r_{ij} is the shortest distance between a backbone bead on nanorod i and a backbone bead on nanorod j, α_{ij} is the angle between the "nanorod vectors" of i and j, defined as pointing from one end to the other end of each nanorod, and $\mathbf{1}_{r_{ij}\le r}$ is the indicator function that is equal to 1 if $r_{ij} \le r$ and 0 otherwise. For small values of r, $S_2(r)$ provides information about local orientational ordering between neighboring nanorods, and at larger values of r, $S_2(r)$ shows how well the short-range orientational order is carried over to longer length scales. If all nanorods within distance of r form a parallel alignment, $S_2(r) = 1$, indicating perfect nematic ordering. If the nanorods are orientationally disordered, $S_2(r)$ approaches zero.

When the nanorods are not dispersed, they could be aggregated into a large phase separated cluster or into many finite-sized clusters or be part of a percolating network. For all three nondispersed nanorod structures, we apply the following procedure to identify the clusters of nanorods. Two nanorods are considered to be in the same cluster if they have at least one pair of beads from each nanorod within $2^{1/6}d$ of each other. Using this criterion and the breadth-first search (BFS) algorithm,[83] we go through all the nanorods and group them into clusters. Then, we investigate percolation in each of the three dimensions (x, y, or z). The morphology is "percolated" if at least one cluster is connected to itself across the boundary of simulation box along one or more dimensions, as in this case the cluster will span infinitely if periodic images are laid out along that (those) dimension(s). We report the total number of percolated dimensions for a specific configuration, ranging from 0 (when no clusters are connected to itself along any of the x, y, and z directions) to 3 (when there is/are cluster(s) connected to itself (themselves) along all three directions).

We also quantify the conformation of the matrix polymer chain by calculating for each chain its squared radius of gyration, R_g^2,

$$R_g^2 = \frac{1}{N}\sum_{i=1}^{N} |\boldsymbol{R}_i - \boldsymbol{R}_{com}|^2 \tag{5}$$

where N is the number of CG beads in the matrix chain, R_i is the coordinate of the ith CG polymer bead, and R_{com} is the coordinate of the center-of-mass of the matrix chain. We report the ensemble average squared radius of gyration, $\langle R_g^2\rangle$, of all the matrix chains in simulation box and $\langle R_g^2\rangle$ of interfacial chains and bulk chains separately. Interfacial chains are matrix chains that have at least one CG matrix bead whose center is within $2^{1/6}d$ of the center of any CG nanorod bead. Bulk chains are matrix chains that have no CG matrix bead whose center is within $2^{1/6}d$ of the center of any CG nanorod bead.

II.D. Parameters Varied. In this paper, the nanorod diameter $D = 1d$, which is the same as the Kuhn length of the matrix polymer, and the nanorod lengths considered are L = 3d, 5d, and 15d. We study three different matrix lengths, N = 1 (equivalent to a small molecule solvent), N = 20, and N = 80. The three nanorod lengths are commensurate with the radius of gyration (R_g) for the 20-mer chain, R_g for the 80-mer chain, and three times the R_g for the 80-mer chain, respectively, giving us a diversified combination of relative length scales between matrix and nanorod. We maintain the total occupied volume fraction in the simulation box, η, defined as $\frac{\text{volume of all matrix CG beads and nanorod CG beads}}{\text{volume of the simulation box}}$, equal to 0.35 to model a melt-like condition. We study three experimentally relevant filler fractions, ϕ_r, defined as $\frac{\text{volume of all nanorod CG beads}}{\text{volume of all matrix CG beads and nanorod CG beads}}$, equal to 0.05, 0.10, and 0.20. We consider two isotropic attraction strengths (ϵ_{iso} = 0.5kT and 1.0kT) and two directional attraction strengths (ϵ_{dir} = 4kT and 8kT).

III. RESULTS AND DISCUSSION

III.A. Comparison between Isotropic and Directional Attraction between Nanorods. In this subsection, we show how the differences in the type of attraction between nanorods

https://dx.doi.org/10.1021/acs.jpcb.1c00097
J. Phys. Chem. B 2021, 125, 2435−2449

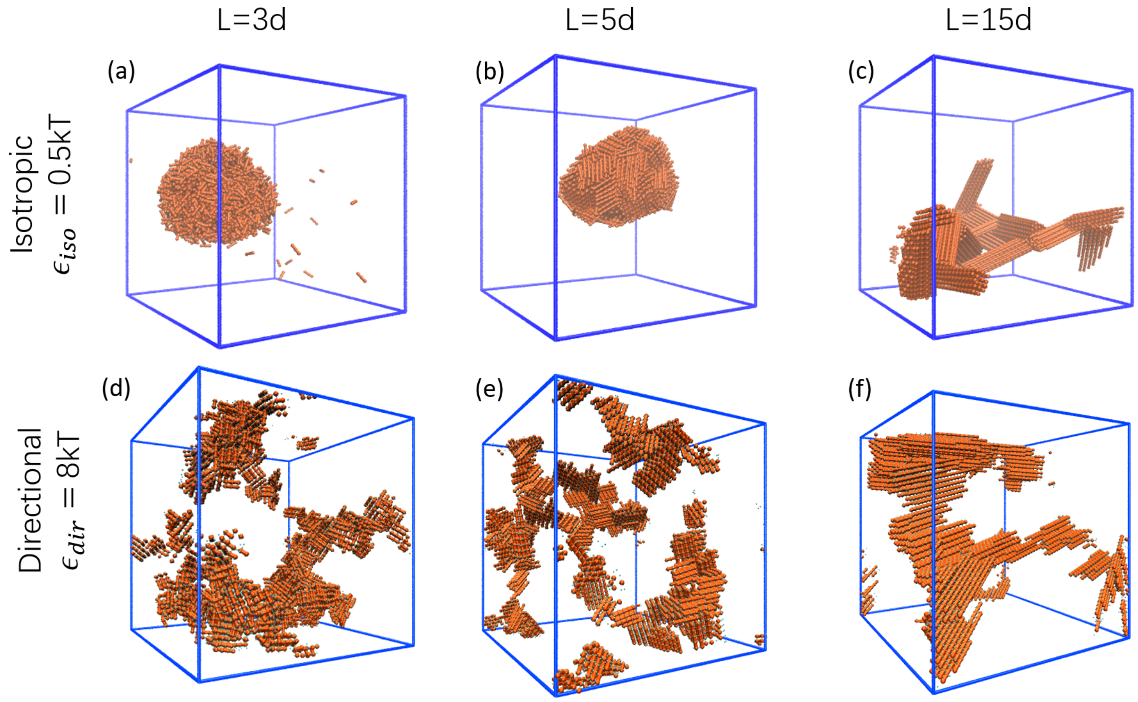

Figure 2. Simulation snapshots of nanorods (matrix chains hidden) obtained using Visual Molecular Dynamics (VMD)[84] for PNCs with $\phi_r = 0.10$, $N = 20$, and (a) $L = 3d$ nanorods with isotropic nanorod−nanorod attraction and $\epsilon_{iso} = 0.5kT$, (b) $L = 5d$ nanorods with isotropic nanorod−nanorod attraction and $\epsilon_{iso} = 0.5kT$, (c) $L = 15d$ nanorods with isotropic nanorod−nanorod attraction and $\epsilon_{iso} = 0.5kT$, (d) $L = 3d$ nanorods with directional nanorod−nanorod attraction and $\epsilon_{dir} = 8kT$, (e) $L = 5d$ nanorods with directional nanorod−nanorod attraction and $\epsilon_{dir} = 8kT$, and (f) $L = 15d$ nanorods with directional nanorod−nanorod attraction and $\epsilon_{dir} = 8kT$. Nanorods are shown in orange, and matrix chains are hidden for clarity.

(arising from, e.g., homogeneous/patchy surface chemistry of nanorod) leads to different morphologies within the PNCs. The nanorod volume fraction of both isotropic and directional PNCs are chosen to be $\phi_r = 0.10$. Based on our calculations of potential of mean force (PMF) between two nanorods (see the Supporting Information, Section SA1), $\epsilon_{iso} = 0.5kT$ for the isotropic model and $\epsilon_{dir} = 8kT$ for the directional model produce similar effective attraction between two nanorods. Therefore, to compare the effect of isotropic and directional interactions between nanorods in PNCs with otherwise identical design parameters, we compare the results for these two interaction strengths: $\epsilon_{iso} = 0.5kT$ for the isotropic model and $\epsilon_{dir} = 8kT$ for the directional model.

We first look at visual characterization of the final structure of the PNCs with nanorods of length $L = 3d$, $5d$, and $15d$. Figure 2 has simulation images only for the PNCs with polymer matrix chain length $N = 20$ and $\phi_r = 0.10$; the representative simulation images for PNCs with $N = 1$ and $N = 80$ at all ϕ_r are in the Supporting Information Figures S6−S11. For $L = 3d$ and $5d$ nanorods, isotropic nanorod−nanorod attraction leads to phase-separated aggregation, while directional nanorod−nanorod attraction drives nanorods into a percolated network structure, comprised of both side-by-side parallel nanorod alignments and side-to-end perpendicular nanorod arrangement. The attractive patches along the nanorod surface in the directional model limit the ways the nanorods can assemble in contrast to the isotropic model, which is homogeneously attractive in all possible directions driving the nanorods into one large cluster. We direct the reader to the Supporting Information, Section SA2, where we show how the isotropic and directional nanorod−nanorod interactions affect the alignment and preferred configurations of two nanorods at close distances. For $L = 15d$ nanorods, with both isotropic and directional attractions, the nanorods align side-by-side and form nanorod bundles that are either finite-sized or percolating in one dimension. For $L = 15d$, the difference in PNC structure with the isotropic and directional models is small, and far less dramatic as compared to that for $L = 3d$ and $5d$. For longer nanorods, the entropically driven depletion effect[85] between nanorods and matrices/solvent beads is dominant, driving the long nanorods to form well aligned aggregates. In later sections, we also compare PNCs of both directional and isotropic models to PNCs in which the nanorods only interact with each other via purely repulsive interactions to show that for $L = 15d$ PNCs the results we see here for these isotropic and directional *attractive* models are similar to those PNCs with repulsive-only interactions. This proves that the enthalpic driving forces are relatively insignificant compared to the entropic driving forces at these relatively high nanorod aspect ratios.

Figure 3 shows the nanorod−nanorod radial distribution functions for all three nanorod lengths and all three solvent/matrix lengths of the isotropic and directional models. For PNCs with isotropic nanorod−nanorod attraction (Figure 3, parts a, c, and e), the contact peak increases with L, showing the increasing contribution of entropically driven depletion effect in addition to the enthalpic effect from nanorod−nanorod attraction. It is also worth noting that nanorods in $N = 1$ solutions in general show a higher contact peak than analogous PNCs with $N = 20$ and 80 matrix chains because the translational entropy gain of the solvent beads upon nanorod aggregation is expected to be larger than the translational entropy gain of the polymer chains. For PNCs with directional nanorod−nanorod attraction (Figure 3b, d, and f), the increase

https://dx.doi.org/10.1021/acs.jpcb.1c00097
J. Phys. Chem. B 2021, 125, 2435−2449

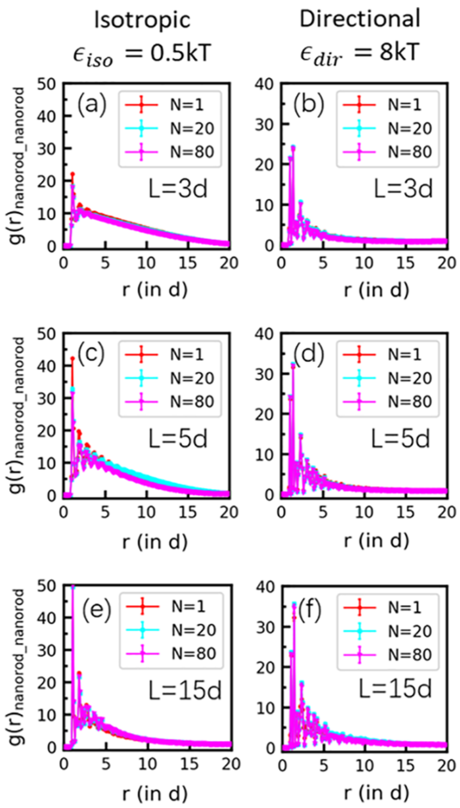

Figure 3. Nanorod−nanorod radial distribution functions, $g(r)_{nanorod-nanorod}$, for PNCs with ϕ_r = 0.10 and (a) L = 3d nanorods with isotropic nanorod−nanorod attraction and ϵ_{iso} = 0.5kT, (b) L = 3d nanorods with directional nanorod−nanorod attraction and ϵ_{dir} = 8kT, (c) L = 5d nanorods with isotropic nanorod−nanorod attraction and ϵ_{iso} = 0.5kT, (d) L = 5d nanorods with directional nanorod−nanorod attraction and ϵ_{dir} = 8kT, (e) L = 15d nanorods with isotropic nanorod−nanorod attraction and ϵ_{iso} = 0.5kT, and (f) L = 15d nanorods with directional nanorod−nanorod attraction and ϵ_{dir} = 8kT. Red represents N = 1, cyan represents N = 20, and pink represents N = 80. Error bars represent the standard deviation from 15 configurations collected from three simulation trials, and when not visible, error bars are smaller than the symbol size.

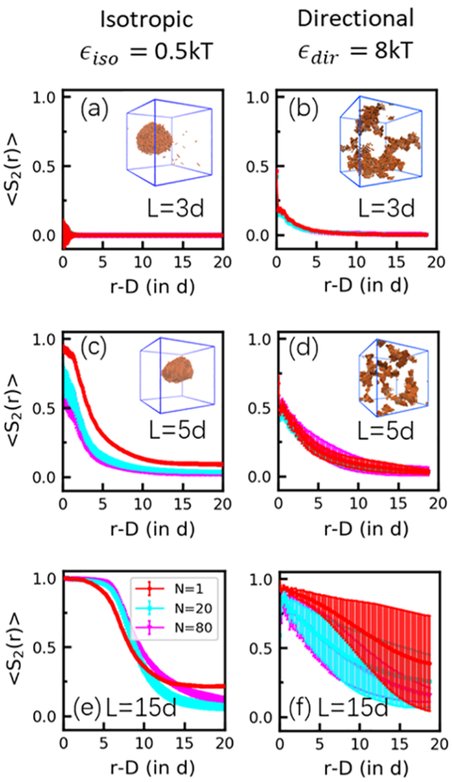

Figure 4. Nanorod orientational order parameter, $\langle S_2(r)\rangle$, for PNCs with ϕ_r = 0.10 and (a) L = 3d nanorods with isotropic nanorod−nanorod attraction and ϵ_{iso} = 0.5kT, (b) L = 3d nanorods with directional nanorod−nanorod attraction and ϵ_{dir} = 8kT, (c) L = 5d nanorods with isotropic nanorod−nanorod attraction and ϵ_{iso} = 0.5kT, (d) L = 5d nanorods with directional nanorod−nanorod attraction and ϵ_{dir} = 8kT, (e) L = 15d nanorods with isotropic nanorod−nanorod attraction and ϵ_{iso} = 0.5kT, and (f) L = 15d nanorods with directional nanorod−nanorod attraction and ϵ_{dir} = 8kT. Red represents N = 1, cyan represents N = 20, and pink represents N = 80. Insets of parts a−d show visualization of an example system of N = 20 at their corresponding attraction type, attraction strength, and nanorod length. The expanded views of these visualizations can be found in Figure 2. Error bars represent the standard deviation from 15 configurations collected from three simulation trials, and when not visible, error bars are smaller than the symbol size.

in contact peak with nanorod length is less significant than that for the analogous isotropic PNCs. The plots for L = 5d (Figure 3d) and L = 15d (Figure 3f) with directional attraction are similar, indicating that with limited possible nanorod packing configurations mainly determined by the placements of interaction sites on the nanorod surface, the local nanorod packing is similar across nanorod lengths. We also note that the first peak in the nanorod−nanorod radial distribution functions seen in the isotropic PNCs "splits" into two discrete and narrow peaks in directional PNCs. This is mainly due to the regularly distanced interaction sites on the nanorod surface in our model, leading to highly refined relative positions between nanorod beads. These sharp discrete peaks can only be seen in experiments if the functional groups or "patches" on the nanorod surface are as perfectly spaced out on nanorod surface as our model. If the patches lack this regular periodicity, then the contact peaks in the radial distribution function for the directional PNCs will be smeared out.

From the plots of orientational order parameter, $\langle S_2(r)\rangle$, in Figure 4, we note that L = 3d PNCs with both isotropic (Figure 4a) and directional (Figure 4b) nanorod−nanorod attractions show a value close to zero over both short and long length scales. However, the corresponding simulation snapshots tell us that this does not mean that both aggregated structures are disordered. For isotropic PNCs, nanorods are randomly oriented (as shown in the visualization in Figure 2a) with $\langle S_2(r)\rangle$ at 0 consistently in both short and long-range. For directional PNCs, nanorods at close distances are highly ordered and exhibit either parallel (α_{ij} = 0 or 180°) or perpendicular alignment (α_{ij} = 90°), leading to P_2 values of 1 and −0.5, respectively, and the average of an ensemble of these two discrete values results in an $\langle S_2(r)\rangle$ value of ~0.2. For L = 5d PNCs, even though the directional and isotropic PNCs show similar values of $\langle S_2(r)\rangle$, we see a cluster of nanorods of finite size with some short-range order for the isotropic PNCs (Figure 4c), and a network structure of parallel and perpendicular alignment of nanorods for the directional PNCs (Figure 4d). For isotropic PNCs, stronger depletion forces induce short-range alignment. For directional PNCs, L = 5d PNCs have a higher occurrence of parallel alignments with directional nanorod−nanorod attraction than L = 3d PNCs, and thus the $\langle S_2(r)\rangle$ value is higher.

https://dx.doi.org/10.1021/acs.jpcb.1c00097
J. Phys. Chem. B 2021, 125, 2435−2449

Table 1. Number of Percolated Dimensions in the Last Configuration for Each Trial and the Average Value of All Three Trials for PNCs with ϕ_r = 0.10

Physical parameters		No. of percolated dimensions Isotropic, 0.5 kT				No. of percolated dimensions Directional, 8 kT			
		Trial 1	Trial 2	Trial 3	Ave.	Trial 1	Trial 2	Trial 3	Ave.
L = 3d	N = 1	0	0	0	**0**	2	2	2	**2**
	N = 20	0	0	0	**0**	0	3	2	**1.67**
	N = 80	0	0	0	**0**	1	3	0	**1.33**
L = 5d	N = 1	0	0	0	**0**	1	1	0	**0.67**
	N = 20	0	0	0	**0**	2	1	1	**1.33**
	N = 80	0	0	0	**0**	0	0	1	**0.33**
L = 15d	N = 1	2	0	0	**0.67**	1	1	1	**1**
	N = 20	1	0	1	**0.67**	1	1	1	**1**
	N = 80	0	0	0	**0**	1	0	0	**0.33**

In contrast to $L = 3d$ and $L = 5d$, in $L = 15d$ PNCs, both directional and isotropic PNCs present ordered bundles of nanorods where parallel (nematic) alignment takes dominance, and thus both $\langle S_2(r)\rangle$ plots (Figure 4, parts e and f) have high values. The $\langle S_2(r)\rangle$ for isotropic PNCs show that the nanorods form nearly perfect short-range order consistently, but it decays more rapidly with distance (Figure 4e), while directional PNCs also show high short-range orientation order with high fluctuation which gradually decays as the distance increases (Figure 4f). With isotropic nanorod–nanorod attractions, the entropic driving forces and enthalpic driving forces align the nanorods at short-range, giving rise to the high $\langle S_2(r)\rangle$ at short r. In contrast, with directional nanorod–nanorod attractions, the nanorod–nanorod attraction is localized to the patches on the nanorod, and the remaining surface of the nanorods are repulsive to each other resulting in frustrations in nanorod–nanorod alignment and increased fluctuations in $\langle S_2(r)\rangle$.

In Table 1, we show the number of percolated dimensions from the last configuration of each of the three independent simulation trials for each PNC. For PNCs with $L = 3d$ or $5d$ nanorods with isotropic attraction, we do not observe any percolation, as they phase separate into a single large cluster of finite size. In contrast, with directional attraction, PNCs with $L = 3d$ or $5d$ nanorods exhibit structures spanning the simulation box and percolating in multiple dimensions. For $L = 15d$ PNCs, both isotropic and directional PNCs form aligned nanorod bundles that extend in one direction, and the number of percolated dimensions, regardless of the nature of attraction, fluctuates around one.

Next, we investigate if and how the matrix chain conformations are perturbed by the addition of nanorods in PNCs. Figure 5 shows the $\langle R_g^2\rangle$ in PNCs with ϕ_r = 0.10 normalized by $\langle R_{g,no\ rod}^2\rangle$ in pure polymer melt (no nanorods) for all the PNCs with matrix chain length N = 20 and N = 80. The $\langle R_g^2\rangle$ for N = 20 and N = 80 neat polymer matrices (from our simulations of polymer chains without nanorods) are $5.35d^2$ and $24.38d^2$, respectively. All PNCs show that interfacial chains, i.e., matrix chains in contact with nanorods, are extended, while bulk chains, or matrix chains without any contact to nanorods, are either contracted or statistically equal to the chain sizes seen in pure polymer melt (no nanorods). As the interfacial chains make up only a small fraction of all chains for this low nanorod volume fraction, the $\langle R_g^2\rangle$ of all chains (i.e., interfacial and bulk together) is statistically similar to that

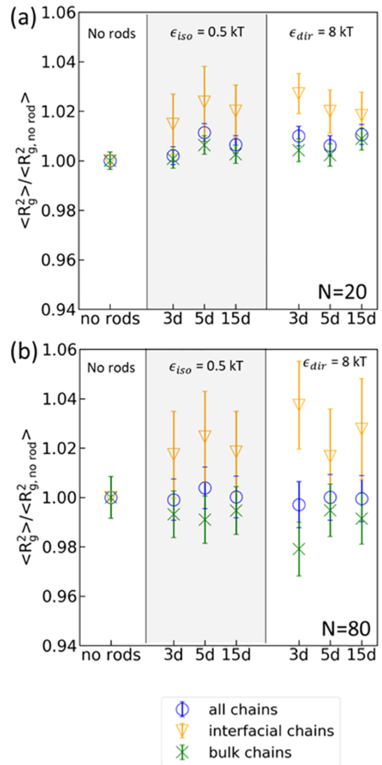

Figure 5. Matrix chains' mean-squared radius of gyration, $\langle R_g^2\rangle$, in PNCs with ϕ_r = 0.10 normalized by $\langle R_g^2\rangle$ in pure polymer melt (no nanorods) for (a) matrix chains of N = 20 and (b) N = 80. The no rods column is the reference $\langle R_{g,no\ rod}^2\rangle$ of the pure melt containing only polymer matrix chains. Error bars indicate a 95% confidence interval for $\langle R_g^2\rangle/\langle R_{g,no\ rod}^2\rangle$ in each PNC.

of the chains in the pure polymer melt. One may expect that the fraction of interfacial chains will depend on the PNC morphology, which is a function of the nanorod volume fraction and the (isotropic and directional) nanorod–nanorod attraction strength. The effects of nanorod volume fraction and nanorod–nanorod attraction strength on the PNC morphology are described next.

III.B. PNCs with Increasing Isotropic Nanorod–Nanorod Attraction Strength. In this subsection, we compare the morphology in PNCs with isotropic nanorod–nanorod

https://dx.doi.org/10.1021/acs.jpcb.1c00097
J. Phys. Chem. B 2021, 125, 2435–2449

repulsion and isotropic nanorod−nanorod attraction strength, ϵ_{iso}, of 0.5kT and 1.0kT at various nanorod volume fractions.

For $L = 3d$ nanorods with repulsive interactions, at all three nanorod volume fractions, ϕ_r = 0.05, 0.10, and 0.20, the nanorods remain dispersed in solvent (N = 1) or polymer matrix (N = 20 and 80); this is shown visually in Figure S6. The nanorod positional and orientational order at ϕ_r = 0.10 are presented in Figure 6, parts a and b. Analogous results at other

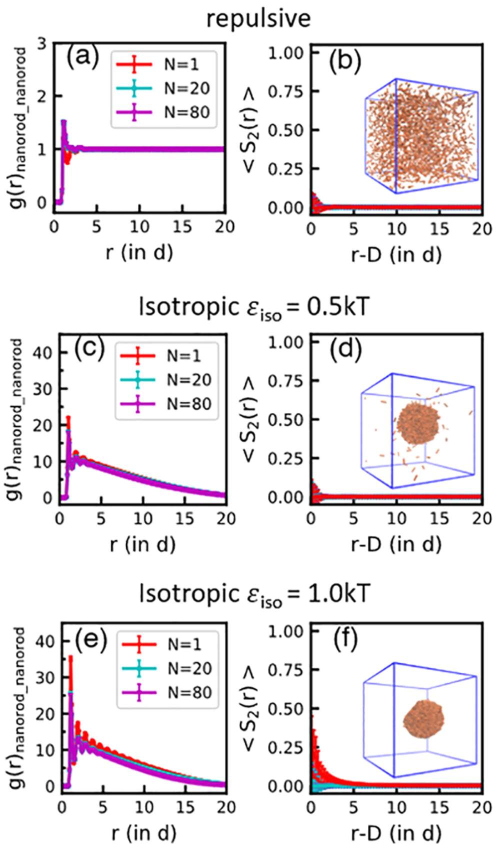

Figure 6. (a, c, e) Nanorod-nanorod radial distribution functions, $g(r)_{nanorod-nanorod}$, of $L = 3d$ PNCs with ϕ_r = 0.10 and (a) repulsive interaction, (c) isotropic nanorod−nanorod attraction, ϵ_{iso} = 0.5kT, and (e) isotropic nanorod−nanorod attraction, ϵ_{iso} = 1.0kT. (b, d, f) Orientational order parameter, $\langle S_2(r)\rangle$, of $L = 3d$ PNCs with ϕ_r = 0.10 and (b) repulsive interaction, (d) isotropic nanorod−nanorod attraction, ϵ_{iso} = 0.5kT, and (f) isotropic nanorod−nanorod attraction, ϵ_{iso} = 1.0kT. Insets in parts b, d, and f show the VMD snapshots of $L = 3d$ nanorods in solvent (N = 1) with solvent beads hidden from view. Error bars represent the standard deviation from 15 configurations collected from three simulation trials, and when not visible, error bars are smaller than the symbol size.

ϕ_r are presented in the Supporting Information, Figures S12 and S13. With repulsive interactions, at all ϕ_r, nanorods maintain fluid-like correlations and have no preferred orientations as the orientational order parameter $\langle S_2(r)\rangle$ is close to 0 at both short-range and long-range (see, for example, Figure 6, parts a and b, for ϕ_r = 0.10.

With isotropic attraction ϵ_{iso} = 0.5kT, at all three ϕ_r, nanorods aggregate into a large cluster and phase separate from matrix chains. The $g(r)_{nanorod-nanorod}$ contact peak in solvent/matrix media increases significantly from that seen in the purely repulsive PNCs (see for example, Figure 6c for ϕ_r = 0.10). The $g(r)_{nanorod-nanorod}$ at different ϕ_r have similar shape with the contact peak being inversely proportional to ϕ_r as expected; at higher ϕ_r, because the bulk number density of the nanorods is higher, the value of $g(r)_{nanorod-nanorod}$ peaks is correspondingly lower. Thus, the local packing among the nanorods does not change with ϕ_r. At all ϕ_r, the nanorods are orientationally disordered with $\langle S_2(r)\rangle$ close to 0 across all length scales (see for example, Figure 6d for ϕ_r = 0.10).

As ϵ_{iso} is increased to 1.0kT, at all ϕ_r, the contact peak in the $g(r)_{nanorod-nanorod}$ increases significantly for $L = 3d$ nanorods in solvent (N = 1) while $g(r)_{nanorod-nanorod}$ only increases slightly in polymer matrix (N = 20, 80). The orientational order of the nanorods at ϵ_{iso} = 1.0kT shows quantitative differences among the three ϕ_r. At ϕ_r = 0.05, there is an observable short-range orientational order in the N = 1 PNCs, indicated by the positive nonzero $\langle S_2(r)\rangle$ at small r in Figure S12f. This is because the solvent (N = 1) beads gain more translation entropy when the nanorods align and order than matrix polymer chains do. This short-range alignment seen for N = 1 solutions with ϕ_r = 0.05 is lowered at ϕ_r = 0.10 (Figure 6f) and disappears for ϕ_r = 0.20 (Figure S13f) as the translation entropy gain of solvent beads upon nanorod ordering decreases as the nanorods volume fraction increases.

In terms of global structure, in all PNCs with $L = 3d$ nanorods, the nanorods either remain dispersed with repulsive nanorod−nanorod interaction or form phase-separated aggregates with isotropic nanorod−nanorod attraction. We do not see any percolation for nanorods with this length in our simulations (see Table 2 for ϕ_r = 0.10 and Tables S3 and S4 for ϕ_r = 0.05 and 0.20, respectively)

For PNCs with $L = 5d$ nanorods, the nanorod positional and orientational order at ϕ_r = 0.10 are presented in Figure 7. Analogous results at other ϕ_r are presented in the Supporting Information, Figures S14 and S15. All the morphologies for $L = 5d$ nanorods are shown visually in Figure S7. We observe (mostly) similar trends in morphology as those seen with $L = 3d$ nanorods. We only highlight the few differences we observe as we go from $L = 3d$ to $L = 5d$. With ϵ_{iso} = 0.5 and 1.0kT, we observe higher short-range orientational order consistently for the $L = 5d$ nanorods as compared to the $L = 3d$ nanorods, at all values of N and ϕ_r. The $\langle S_2(r)\rangle$ plots (Figure 7d) show a higher short-range orientational order for N = 1 than N = 20 or 80 at ϵ_{iso} = 0.5 kT; this is for the same entropic reasons stated for $L = 3d$ at ϵ_{iso} = 1.0 kT. The orientational order for $L = 5d$ nanorods at ϵ_{iso} = 1.0 kT (Figure 7f) becomes similar for all values of N due to stronger enthalpic driving forces toward nanorod aggregation and alignment.

For PNCs with $L = 15d$ nanorods, the nanorod positional and orientational order at ϕ_r = 0.10 are presented in Figure 8. Analogous results at other ϕ_r are presented in the Supporting Information, Figures S16 and S17, and all the morphologies are shown visually in Figure S8. With purely repulsive interaction between $L = 15d$ nanorods, at all three ϕ_r, the entropic driving forces lead to high nanorod short-range orientational order within aggregated bundles at all values of N (see for example, Figure 8b for ϕ_r = 0.10). The bundles formed in solvent or polymer matrix only differ slightly in structure. The visuals of the morphology in Figure S8 show that in solvent (N = 1), nanorods form finite size bundles at low ϕ_r and a connected bundles structure at ϕ_r = 0.20, with high long-range orientational order. The structures in polymer matrix (N = 20 and 80) are similar to that in solvent. However, we expect the gain in the translational entropy of the polymer chains upon aggregation of nanorods should be less significant than

https://dx.doi.org/10.1021/acs.jpcb.1c00097
J. Phys. Chem. B 2021, 125, 2435−2449

Table 2. Number of Percolated Dimensions for Each Simulation Trial at ϕ_r = 0.10 Compared in This Section[a]

Physical parameters		No. of percolated dimensions Repulsive				No. of percolated dimensions Isotropic, 0.5kT				No. of percolated dimensions Isotropic, 1.0kT			
		Trial 1	Trial 2	Trial 3	Ave.	Trial 1	Trial 2	Trial 3	Ave.	Trial 1	Trial 2	Trial 3	Ave.
L = 3d	N = 1	0	0	0	**0**	0	0	0	**0**	0	0	0	**0**
	N = 20	0	0	0	**0**	0	0	0	**0**	0	0	0	**0**
	N = 80	0	0	0	**0**	0	0	0	**0**	0	0	0	**0**
L = 5d	N = 1	0	0	0	**0**	0	0	0	**0**	0	0	0	**0**
	N = 20	0	0	0	**0**	0	0	0	**0**	0	0	0	**0**
	N = 80	0	0	0	**0**	0	0	0	**0**	0	0	0	**0**
L = 15d	N = 1	0	0	0	**0**	2	0	0	**0.67**	2	1	1	**1.33**
	N = 20	0	0	0	**0**	1	0	1	**0.67**	0	1	0	**0.33**
	N = 80	0	0	0	**0**	0	0	0	**0**	1	0	0	**0.33**

[a]An average number of percolated dimensions is calculated as an average of all three trials for each PNC.

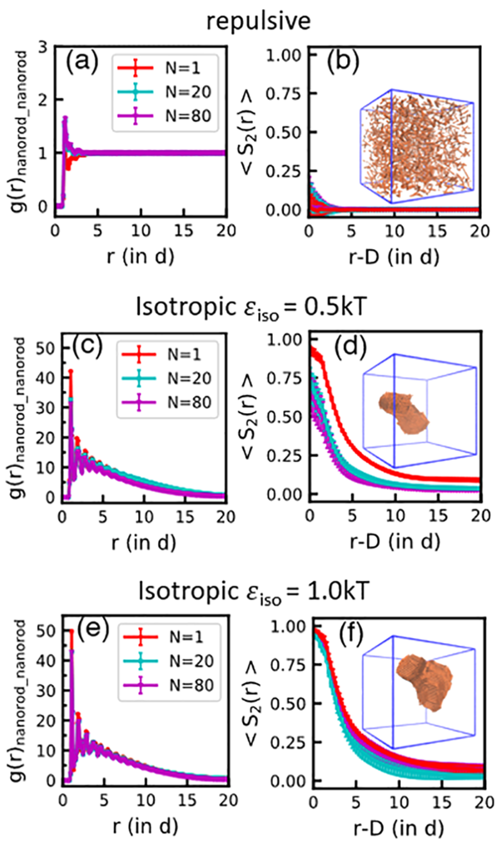

Figure 7. (a, c, e) Nanorod−nanorod radial distribution functions, $g(r)_{nanorod-nanorod}$, of L = 5d PNCs with ϕ_r = 0.10 and with (a) repulsive interaction, (c) isotropic nanorod−nanorod attraction, ϵ_{iso} = 0.5 kT, and (e) isotropic nanorod−nanorod attraction, ϵ_{iso} = 1.0 kT. (b, d, f) Orientational order parameter, $\langle S_2(r)\rangle$, of L = 5d PNCs with ϕ_r = 0.10 and (b) repulsive interaction, (d) isotropic nanorod−nanorod attraction, ϵ_{iso} = 0.5 kT, and (f) isotropic nanorod−nanorod attraction, ϵ_{iso} = 1.0 kT. Insets in parts b, d, and f show the VMD snapshots of L = 5d nanorods in solvent (N = 1) with solvent beads hidden from view. Error bars represent the standard deviation from 15 configurations collected from three simulation trials, and when not visible, error bars are smaller than the symbol size.

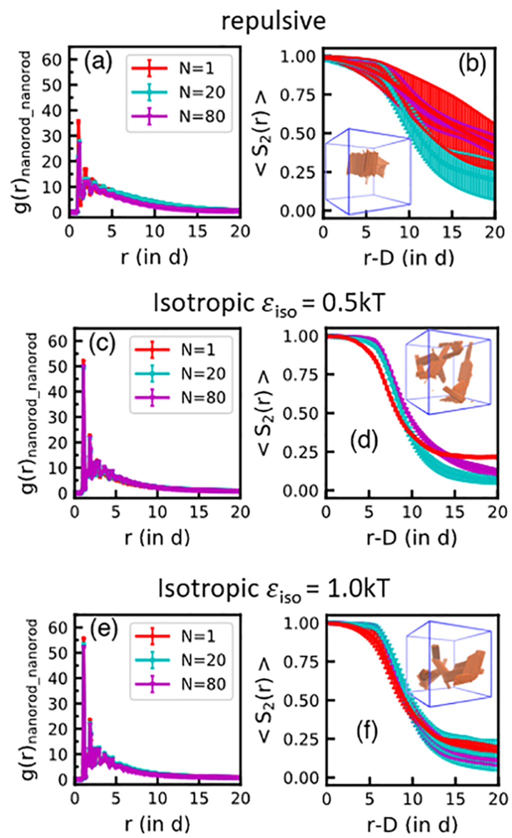

Figure 8. (a, c, e) Nanorod-nanorod radial distribution functions, $g(r)_{nanorod-nanorod}$, of L = 15d PNCs with ϕ_r = 0.10 and (a) repulsive interaction, (c) isotropic nanorod−nanorod attraction, ϵ_{iso} = 0.5 kT, and (e) isotropic nanorod−nanorod attraction, ϵ_{iso} = 1.0 kT. (b, d, f) Orientational order parameter, $\langle S_2(r)\rangle$, of L = 15d PNCs with ϕ_r = 0.10 and (b) repulsive interaction, (d) isotropic nanorod−nanorod attraction, ϵ_{iso} = 0.5 kT, and (f) isotropic nanorod−nanorod attraction, ϵ_{iso} = 1.0 kT. Insets in parts b, d, and f show the VMD snapshots of L = 15d nanorods in solvent (N = 1) with solvent beads hidden from view. Error bars represent the standard deviation from 15 configurations collected from three simulation trials, and when not visible, error bars are smaller than the symbol size.

that of the solvent (N = 1) beads; thus, the driving force for nanorod aggregation should be weaker. This is confirmed quantitatively by the $g(r)_{nanorod-nanorod}$ contact peaks being higher in the solvent as compared to the polymer matrix at all

ϕ_r (see for example, Figure 8a for $\phi_r = 0.10$). We do not see percolation for any of the N or ϕ_r for PNCs with $L = 15d$ nanorods (see Table 2 for $\phi_r = 0.10$ and Tables S3 and S4 for $\phi_r = 0.05$ and 0.20, respectively).

With isotropic attraction, the overall morphology of the PNCs with $L = 15d$ remains qualitatively the same as that seen with repulsive-only interactions. At $\phi_r = 0.10$, $\epsilon_{iso} = 0.5\ kT$, and $\epsilon_{iso} = 1.0\ kT$, the $g(r)_{nanorod-nanorod}$ contact peak in all three media (Figure 8, parts c and e) increases from that in the purely repulsive PNCs and any differences seen between the solvent/polymer matrix PNCs are removed. High short-range orientational order is seen at all ϕ_r at $\epsilon_{iso} = 0.5\ kT$ and $\epsilon_{iso} = 1.0\ kT$. When ϵ_{iso} increases from $0.5kT$ to $1.0kT$, at all ϕ_r, unlike $L = 3d$ or $L = 5d$ cases, there is no further increase in the values of $g(r)_{nanorod-nanorod}$ peaks. The percolation number generally increases with ϕ_r and is not dependent on ϵ_{iso}. At $\phi_r = 0.05$, we see nearly no percolation (Table S3), but at $\phi_r = 0.10$, we see percolation in one-dimension. (Table 2) At $\phi_r = 0.20$, we see high percolation number in both the solvent and the $N = 20$ polymer matrix while the percolation number of the $N = 80$ matrix system is low (Table S4).

Lastly, with regards to the chain conformations, in the Supporting Information, Figures S24−S26, we show the interfacial or bulk chains' conformations as a function of nanorod volume fraction for PNCs with isotropic nanorod−nanorod attraction. Regardless of nanorod length or isotropic nanorod−nanorod attraction strength, we see the same behavior described in Section III.A, where the interfacial chains extend and the bulk chains remain mostly unperturbed or slightly contract in some cases, resulting in all chains being unperturbed on average. Despite the different morphologies adopted by 5−20 vol % nanorods and the likely differences in the polymer−nanorod interfacial area, we do not observe a dependence of the change in the polymer matrix chain conformation on the PNC morphology when the matrix−nanorod interaction is athermal.

III.C. PNCs with Increasing Directional Nanorod−Nanorod Attraction Strength. In this subsection, we show the effect of *directional* nanorod−nanorod attraction strength and nanorod volume fraction on the PNC morphology. In section III.B, we presented the PNC morphologies for repulsive-only nanorod−nanorod interactions and how they changed with increasing *isotropic* nanorod−nanorod attraction strength. Here, we will use the same set of repulsive-only nanorod−nanorod interaction results as a baseline and increase the directional attraction strength to $\epsilon_{dir} = 4kT$ and $8kT$.

In section III.B we showed that for $L = 3d$ nanorods with repulsive interactions, at all volume fractions ($\phi_r = 0.05$, 0.10 and 0.20) and solvent/matrix lengths ($N = 1$, 20, and 80) the nanorods remain dispersed, and nanorod alignment is completely random. We show in Figure 9 the results for $L = 3d$ PNCs with $\phi_r = 0.10$ and $N = 20$ with directional attraction strength between nanorods. The analogous results for $L = 3d$ PNCs at other values of ϕ_r and N are provided in the Supporting Information, Figures S9, S18, and S19.

For $L = 3d$, at all three ϕ_r, the contact peaks of $g(r)_{nanorod-nanorod}$ at $\epsilon_{dir} = 4kT$ only increase slightly from those with repulsive interactions. These results imply that for $L = 3d$ the attraction strength of $\epsilon_{dir} = 4kT$ is not strong enough to compensate for change in entropy in the system upon aggregation. When directional attraction is set to $\epsilon_{dir} = 8kT$, $L = 3d$ nanorods aggregate and form a network structure. At all three ϕ_r, the value of N does not change $g(r)_{nanorod-nanorod}$, as the enthalpic driving force from directional attractions takes dominance in these cases. We remind the reader that when nanorods form network structure comprised of side-by-side and side-to-end nanorod packing, the orientational order parameter $(S_2(r))$ is not meaningful. As for the global structure, at $\epsilon_{dir} = 8kT$, we observe no percolation as the nanorods remain dispersed (see Tables S5−S7). At $\epsilon_{dir} = 8kT$, unlike the PNCs of $L = 3d$ nanorods with *isotropic* attractions where phase-separated aggregation is formed, the network structure driven by directional nanorod−nanorod attractions inherently has a higher tendency to percolate across simulation box. As nanorod volume fraction increases from $\phi_r = 0.05$ to 0.20, the number of percolated dimensions steadily increases.

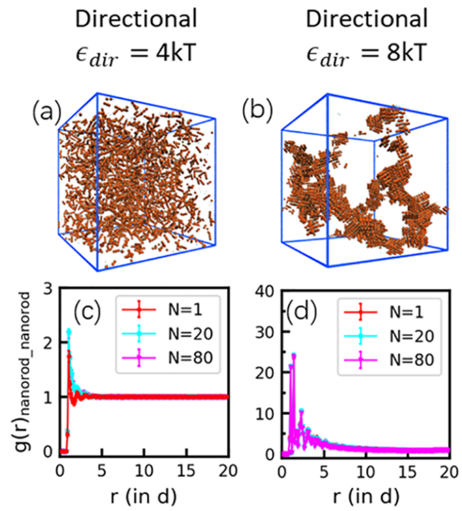

Figure 9. Visualization of simulation configuration and nanorod−nanorod radial distribution functions, $g(r)_{nanorod-nanorod}$ of $L = 3d$ PNCs with $\phi_r = 0.10$, $N = 20$ with directional attraction strength between nanorods (a and c) $\epsilon_{dir} = 4kT$ and (b and d) $\epsilon_{dir} = 8kT$. Error bars represent the standard deviation from 15 configurations collected from three simulation trials, and when not visible, the error bars are smaller than the symbol size.

For $L = 5d$ nanorods, we show in Figure 10 the results for $\phi_r = 0.10$ and $N = 20$ with directional attraction between nanorods. The analogous results for $L = 5d$ PNCs at other values of ϕ_r and N are provided in the Supporting Information, Figures S10, S20 and S21. With the repulsive nanorod−nanorod interaction, the nanorods remain dispersed at all ϕ_r and N. When the directional attraction is set to $\epsilon_{dir} = 4kT$, for all three ϕ_r at $L = 5d$ nanorods already aggregate and form the network structure. We note that this is dramatically different from morphologies of $L = 3d$ nanorods at the same ϵ_{dir}. These contrasting morphologies show the complex interplay between nanorod length and directional attraction strength and how a minor change in nanorod length can change the expected morphology when nanorods have patches that directionally attract each other. At $\epsilon_{dir} = 4kT$, there is no significant difference in $g(r)_{nanorod-nanorod}$ between different matrix/solvent media at each ϕ_r, and the heights of contact peak are, again, inversely proportional to ϕ_r, suggesting similar local packing at different nanorod volume fractions. At $\epsilon_{dir} = 8kT$, there is no significant further change in either visualized morphology or $g(r)_{nanorod-nanorod}$ beyond what we see at $\epsilon_{dir} = 4kT$, suggesting that the effect of the enthalpic gain from the attractive patches coming into contact to drive nanorod aggregation does not change beyond $4kT$. In contrast, in the case of isotropic

https://dx.doi.org/10.1021/acs.jpcb.1c00097
J. Phys. Chem. B 2021, 125, 2435−2449

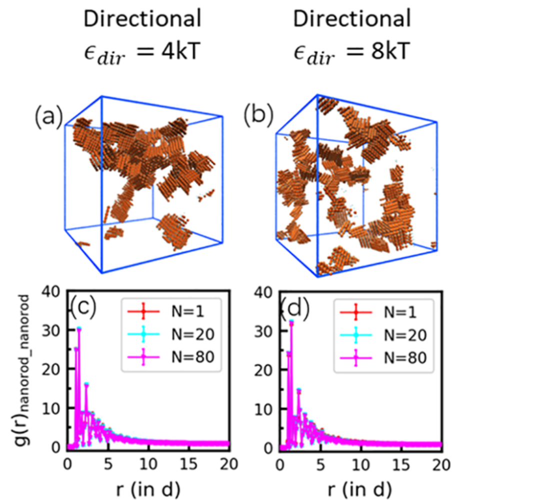

Figure 10. Visualization of simulation configuration and nanorod−nanorod radial distribution functions, $g(r)_{nanorod-nanorod}$, for $L = 5d$ PNCs with $\phi_r = 0.10$, $N = 20$ with directional attraction strength between nanorods (a and c) $\epsilon_{dir} = 4kT$ and (b and d) $\epsilon_{dir} = 8kT$. Error bars represent the standard deviation from 15 configurations collected from three simulation trials, and when not visible, the error bars are smaller than the symbol size.

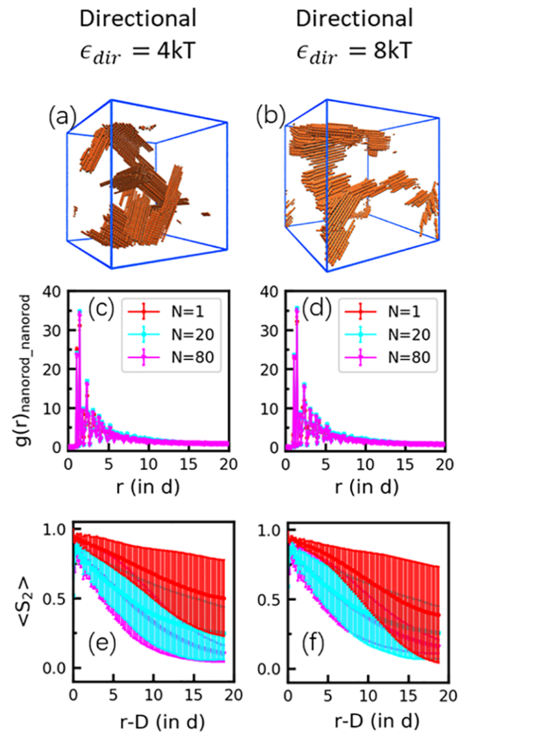

Figure 11. Visualization of simulation configuration, nanorod−nanorod radial distribution functions, $g(r)_{nanorod-nanorod}$, and nanorod orientational order parameters, $\langle S_2(r)\rangle$, for $L = 15d$ PNCs with $\phi_r = 0.10$, $N = 20$ with directional attraction strength between nanorods (a, c, e) $\epsilon_{dir} = 4kT$ and (b, d, f) $\epsilon_{dir} = 8kT$. Error bars represent the standard deviation from 15 configurations collected from three simulation trials, and when not visible, the error bars are smaller than the symbol size.

attraction at analogous nanorod length, we continue to observe quantitative changes in the $g(r)_{nanorod-nanorod}$ contact peak height when ϵ_{iso} increases.

As for the global structure, at $\epsilon_{dir} = 8kT$, with $L = 5d$ nanorods, we see similar number of percolated dimensions as we did for analogous nanorod volume fractions at $\epsilon_{dir} = 8kT$ with $L = 3d$ nanorods. At $\epsilon_{dir} = 4kT$, there is no significant difference in terms of number of percolated dimensions compared to $\epsilon_{dir} = 8kT$ and $\phi_r = 0.10$ or $\phi_r = 0.20$, consistent with the similarity we observed in visualized morphologies and local crowding at these two attraction strengths. Interestingly, at $\phi_r = 0.05$, $L = 5d$ nanorods form some percolation at $\epsilon_{dir} = 8kT$ but not at $\epsilon_{dir} = 4kT$. This result is remarkable as the visualized morphologies (Figure S10) do not show any significant difference between the two directional attraction strengths at $L = 5d$, $\phi_r = 0.05$, and the difference in percolation results seems to suggest that at these low ϕ_r, ϵ_{dir} of 4kT is strong enough to maintain the local assembly structure but not enough to support the network structure of nanorods spanning the entire simulation box, and thus, the nanorods break down into several smaller disconnected assemblies.

For $L = 15d$ nanorods, we show in Figure 11 the results for $\phi_r = 0.10$ and $N = 20$ with directional attraction strength between nanorods. The analogous results for $L = 15d$ PNCs at other values of ϕ_r and N are provided in the Supporting Information Figures S11, S22, and S23. The $L = 15d$ nanorods form bundles with high orientational order with repulsive nanorod−nanorod interaction due to the dominant entropic driving forces. The one-dimensional bundled structure persists when directional attraction is set to $\epsilon_{dir} = 4kT$ at all ϕ_r (see visuals in Figure S11), where the side-by-side packing between nanorods dominate, and we see no signs of side-to-end packing that was prevalent in analogous systems with $L = 3d$ and $5d$ nanorods. At all ϕ_r, the contact peak heights in the nanorod radial distribution functions increase only slightly for $\epsilon_{dir} = 4kT$ from the analogous system with repulsive nanorod−nanorod interactions, confirming that the nanorod aggregation is mainly driven entropically and the directional attractions only play a minor role.

At $\epsilon_{dir} = 4kT$, for most values of ϕ_r and N, for $L = 15d$ nanorods, we see the presence of a strong short-range orientational order that gradually decays as r increases, with significant fluctuations in the value of S_2. There is a notable exception, namely at $\phi_r = 0.05$ and $N = 1$ (Supporting Information Figure S22e), where the nanorods form aggregates with high orientational order at both short-range and long-range. The solvent beads gain more translational entropy upon aggregation of nanorods than the matrix chains ($N = 20$ and 80) do, and thus, the driving force for nanorod aggregation is also stronger for the solvent. When ϵ_{dir} is increased to 8kT, we do not observe any significant difference in visualized morphology, $g(r)_{nanorod-nanorod}$, and $\langle S_2(r)\rangle$ for the $L = 15d$ nanorods compared to analogous systems with $\epsilon_{dir} = 4kT$. There is no significant difference in terms of number of percolated dimensions between the two directional nanorod−nanorod attraction strengths at the same ϕ_r. The number of percolated dimensions for $L = 15d$ nanorods fluctuate around 1 at $\phi_r = 0.05$ and 0.10, agreeing with the mostly one-dimensional bundles we observe in the morphologies. At $\phi_r = 0.20$, we observe some multidimensional percolations due to increased nanorod volume fraction.

Lastly, in the Supporting Information, Figures S27−S29, we show the interfacial or bulk chains' conformations as a function of nanorod volume fraction for PNCs with directional nanorod−nanorod attraction. We see the same trends as we described in Sections III.A and III.B, where the interfacial chains extend and the bulk chains remain mostly unperturbed or slightly contract in some cases, resulting in all chains being unperturbed on average.

Overall, at the relative "short" nanorod lengths ($L = 3d$ and $5d$), with isotropic nanorod−nanorod attractions we observe phase separation, and with directional nanorod−nanorod attraction (when the attraction is strong enough), we observe network structure spanning the entire simulation box, leading to multidimensional percolation when the nanorod volume fraction is high enough. This suggests that for nanorods with short length, heterogeneous/patchy surface chemistry and resulting directional/specific attractions between nanorods can significantly facilitate formation of percolating nanorod structures in PNCs. For long ($L = 15d$) nanorods, the nanorods always form one-dimensional bundles with high orientational order regardless of the type of attraction, signaling dominance of entropic driving forces.

IV. CONCLUSION

In this work, we perform coarse-grained (CG) molecular dynamics (MD) simulations to elucidate the morphology of polymer nanocomposites (PNCs) containing nanorods with two different types of nanorod surface chemistry/functionalization: homogeneous or patchy. The homogeneously functionalized nanorod is modeled as a rigid body of CG nanorod beads interacting with other CG nanorod beads via an isotropic attraction. The patchy functionalized nanorod is modeled as a rigid body of CG nanorod beads with a finite number of attraction sites embedded in the CG nanorod beads that interact with other attraction sites via an effectively directional interaction. In this study, we only consider PNCs where the nanorod diameter is equal to the Kuhn length of the polymer matrix, the nanorod−nanorod interactions are dominant and effectively attractive or repulsive, and all other pairwise interactions (e.g., matrix−matrix or nanorod-matrix) are treated as being purely repulsive. Using CGMD simulations, we study the effect of the type of nanorod surface functionalization, isotropic/directional attraction strength, nanorod dimensions, matrix chain length, and nanorod volume fraction on the morphology of the PNC.

For short nanorods, at similar *effective* nanorod−nanorod attractions, the patchy nanorod surface functionalization leads to a percolated nanorod morphology within the PNC, while homogeneous nanorod surface functionalization leads to a phase-separated aggregate of nanorods. For long nanorods, regardless of the type of nanorod surface functionalization, nanorods form either finite-sized or percolating aggregates/bundles with high short-range orientational order.

How the attraction strength between nanorods affects the morphology is also found to be dependent on whether the nanorod has a homogeneous or patchy functionalization. For homogeneously functionalized nanorods, at all aspect ratios explored (i.e., L/D = 3, 5 and 15), as the isotropic attraction strength increases, the morphology remains qualitatively unchanged, yet the nanorod−nanorod contact peak increases and nanorod orientational order increases. For patchy functionalized nanorods and smaller aspect ratios (i.e., L/D = 3) as the directional attractive strength increases, the PNC morphology goes from dispersed nanorods to percolated nanorods. The $L = 5d$ nanorods consistently form a percolating network structure, while $L = 15d$ nanorods consistently form finite-sized or percolating, one-dimensional bundles.

We also probe the impact of the addition of nanorods on the conformation of matrix chains. At nanorod volume fractions of 0.05, 0.10, and 0.20, regardless of the nanorod surface functionalization, the conformation of all the matrix chains on average remains the same as the matrix chains in a pure melt (with no nanorods). However, this is a cumulative effect of the interfacial chains (i.e., chains in contact with the nanorods) being extended and the bulk chains (i.e., chains far from nanorods) either being compacted or remaining statistically the same as the matrix chains in pure melt. We note that as nanorods and matrix chains interact via purely repulsive potential, any observed perturbation of matrix conformation originates purely from the physical presence and arrangement of nanorods. It will be interesting to study how the morphology (i.e., nanorod arrangement as well as matrix chain conformations) is altered when we consider isotropic vs directional attractive interactions between nanorod and matrix chains.

■ ASSOCIATED CONTENT

Supporting Information

The Supporting Information is available free of charge at https://pubs.acs.org/doi/10.1021/acs.jpcb.1c00097.

Potential of mean force (PMF) calculations between nanorods with isotropic and directional/patchy attractions in a "vacuum" (without solvent/matrix), additional details on simulation protocols, and additional results from CG simulations of PNCs with nanorods (PDF)

■ AUTHOR INFORMATION

Corresponding Author

Arthi Jayaraman − *Department of Chemical and Biomolecular Engineering and Department of Materials Science and Engineering, University of Delaware, Newark, Delaware 19716, United States;* orcid.org/0000-0002-5295-4581; Email: arthij@udel.edu

Authors

Shizhao Lu − *Department of Chemical and Biomolecular Engineering, University of Delaware, Newark, Delaware 19716, United States*

Zijie Wu − *Department of Chemical and Biomolecular Engineering, University of Delaware, Newark, Delaware 19716, United States*

Complete contact information is available at: https://pubs.acs.org/10.1021/acs.jpcb.1c00097

Author Contributions

#S.L. and Z.W. made equal contributions.

Notes

The authors declare no competing financial interest.

■ ACKNOWLEDGMENTS

The authors acknowledge financial support from the U.S. National Science Foundation, Grant NSF DMREF #1921871. The computational work in this study was supported by the Farber High-Performance Supercomputing Center and Caviness High-Performance Computing Community Cluster at the University of Delaware, and Stampede2 Supercomputing Cluster at the Texas Advanced Computing Center (TACC) supported by the Extreme Science and Engineering Discovery Environment (XSEDE).

■ REFERENCES

(1) Balazs, A. C.; Emrick, T.; Russell, T. P. Nanoparticle polymer composites: Where two small worlds meet. *Science* **2006**, *314* (5802), 1107−1110.
(2) Moniruzzaman, M.; Winey, K. I. Polymer nanocomposites containing carbon nanotubes. *Macromolecules* **2006**, *39* (16), 5194−5205.
(3) Tjong, S. C. Structural and mechanical properties of polymer nanocomposites. *Mater. Sci. Eng., R* **2006**, *53* (3−4), 73−197.
(4) Vaia, R. A.; Maguire, J. F. Polymer nanocomposites with prescribed morphology: going beyond nanoparticle-filled polymers. *Chem. Mater.* **2007**, *19* (11), 2736−2751.
(5) Jancar, J.; Douglas, J. F.; Starr, F. W.; Kumar, S. K.; Cassagnau, P.; Lesser, A. J.; Sternstein, S. S.; Buehler, M. J. Current issues in research on structure-property relationships in polymer nanocomposites. *Polymer* **2010**, *51* (15), 3321−3343.
(6) Kumar, S. K.; Krishnamoorti, R. Nanocomposites: Structure, phase behavior, and properties. *Annu. Rev. Chem. Biomol. Eng.* **2010**, *1*, 37−58.
(7) Hore, M. J. A.; Composto, R. J. Functional polymer nanocomposites enhanced by nanorods. *Macromolecules* **2014**, *47* (3), 875−887.
(8) Mutiso, R. M.; Winey, K. I. Electrical properties of polymer nanocomposites containing rod-like nanofillers. *Prog. Polym. Sci.* **2015**, *40* (1), 63−84.
(9) Wang, R.; Chen, C.; Zheng, Y.; Wang, H.; Liu, J.-W.; Yu, S.-H. Structure−property relationship of assembled nanowire materials. *Materials Chemistry Frontiers* **2020**, *4* (10), 2881−2903.
(10) Scotti, R.; Conzatti, L.; D'Arienzo, M.; Di Credico, B.; Giannini, L.; Hanel, T.; Stagnaro, P.; Susanna, A.; Tadiello, L.; Morazzoni, F. Shape controlled spherical (0D) and rod-like (1D) silica nanoparticles in silica/styrene butadiene rubber nanocomposites: Role of the particle morphology on the filler reinforcing effect. *Polymer* **2014**, *55* (6), 1497−1506.
(11) Tadiello, L.; D'Arienzo, M.; Di Credico, B.; Hanel, T.; Matejka, L.; Mauri, M.; Morazzoni, F.; Simonutti, R.; Spirkova, M.; Scotti, R. The filler−rubber interface in styrene butadiene nanocomposites with anisotropic silica particles: morphology and dynamic properties. *Soft Matter* **2015**, *11* (20), 4022−4033.
(12) Du, F.; Scogna, R. C.; Zhou, W.; Brand, S.; Fischer, J. E.; Winey, K. I. Nanotube networks in polymer nanocomposites: Rheology and electrical conductivity. *Macromolecules* **2004**, *37* (24), 9048−9055.
(13) Sun, Y. L.; Tang, H. Y.; Ribbe, A.; Duzhko, V.; Woodard, T. L.; Ward, J. E.; Bai, Y.; Nevin, K. P.; Nonnenmann, S. S.; Russell, T.; Emrick, T.; Lovley, D. R. Conductive Composite Materials Fabricated from Microbially Produced Protein Nanowires. *Small* **2018**, *14* (44), 1802624.
(14) Liu, W.; Lee, S. W.; Lin, D.; Shi, F.; Wang, S.; Sendek, A. D.; Cui, Y. Enhancing ionic conductivity in composite polymer electrolytes with well-aligned ceramic nanowires. *Nature Energy* **2017**, *2* (5), 1−7.
(15) Huang, H.; Liu, C.; Wu, Y.; Fan, S. Aligned carbon nanotube composite films for thermal management. *Adv. Mater.* **2005**, *17* (13), 1652−1656.
(16) Yao, Y.; Zhu, X.; Zeng, X.; Sun, R.; Xu, J.-B.; Wong, C.-P. Vertically aligned and interconnected SiC nanowire networks leading to significantly enhanced thermal conductivity of polymer composites. *ACS Appl. Mater. Interfaces* **2018**, *10* (11), 9669−9678.
(17) Yu, Y.-Y.; Chang, S.-S.; Lee, C.-L.; Wang, C. C. Gold nanorods: electrochemical synthesis and optical properties. *J. Phys. Chem. B* **1997**, *101* (34), 6661−6664.
(18) Murphy, C. J.; Sau, T. K.; Gole, A. M.; Orendorff, C. J.; Gao, J.; Gou, L.; Hunyadi, S. E.; Li, T. Anisotropic metal nanoparticles: Synthesis, assembly, and optical applications. *J. Phys. Chem. B* **2005**, *109* (29), 13857−13870.
(19) Chen, H.; Shao, L.; Li, Q.; Wang, J. Gold nanorods and their plasmonic properties. *Chem. Soc. Rev.* **2013**, *42* (7), 2679−2724.
(20) González-Rubio, G.; Kumar, V.; Llombart, P.; Díaz-Núñez, P.; Bladt, E.; Altantzis, T.; Bals, S.; Peña-Rodríguez, O.; Noya, E. G.; MacDowell, L. G.; et al. Disconnecting symmetry breaking from seeded growth for the reproducible synthesis of high quality gold nanorods. *ACS Nano* **2019**, *13* (4), 4424−4435.
(21) Szustakiewicz, P.; Kowalska, N.; Grzelak, D.; Narushima, T.; Góra, M.; Bagiński, M.; Pociecha, D.; Okamoto, H.; Liz-Marzán, L. M.; Lewandowski, W. Supramolecular Chirality Synchronization in Thin Films of Plasmonic Nanocomposites. *ACS Nano* **2020**, *14* (10), 12918−12928.
(22) Karatrantos, A.; Composto, R. J.; Winey, K. I.; Clarke, N. Structure and conformations of polymer/SWCNT nanocomposites. *Macromolecules* **2011**, *44* (24), 9830−9838.
(23) Glova, A. D.; Falkovich, S. G.; Larin, S. V.; Mezhenskaia, D. A.; Lukasheva, N. V.; Nazarychev, V. M.; Tolmachev, D. A.; Mercurieva, A. A.; Kenny, J. M.; Lyulin, S. V. Poly (lactic acid)-based nanocomposites filled with cellulose nanocrystals with modified surface: all-atom molecular dynamics simulations. *Polym. Int.* **2016**, *65* (8), 892−898.
(24) Khani, S.; Jamali, S.; Boromand, A.; Hore, M. J. A.; Maia, J. Polymer-mediated nanorod self-assembly predicted by dissipative particle dynamics simulations. *Soft Matter* **2015**, *11* (34), 6881−6892.
(25) Shen, J.; Li, X.; Shen, X.; Liu, J. Insight into the Dispersion Mechanism of Polymer-Grafted Nanorods in Polymer Nanocomposites: A Molecular Dynamics Simulation Study. *Macromolecules* **2017**, *50* (2), 687−699.
(26) Chen, Y.; Xu, Q.; Jin, Y.; Qian, X.; Liu, L.; Liu, J.; Ganesan, V. Design of End-to-End Assembly of Side-Grafted Nanorods in a Homopolymer Matrix. *Macromolecules* **2018**, *51* (11), 4143−4157.
(27) Toepperwein, G. N.; Karayiannis, N. C.; Riggleman, R. A.; Kröger, M.; De Pablo, J. J. Influence of nanorod inclusions on structure and primitive path network of polymer nanocomposites at equilibrium and under deformation. *Macromolecules* **2011**, *44* (4), 1034−1045.
(28) Toepperwein, G. N.; Riggleman, R. A.; De Pablo, J. J. Dynamics and deformation response of rod-containing nanocomposites. *Macromolecules* **2012**, *45* (1), 543−554.
(29) Karatrantos, A.; Composto, R. J.; Winey, K. I.; Clarke, N. Nanorod Diffusion in Polymer Nanocomposites by Molecular Dynamics Simulations. *Macromolecules* **2019**, *52* (6), 2513−2520.
(30) Surve, M.; Pryamitsyn, V.; Ganesan, V. Dispersion and percolation transitions of nanorods in polymer solutions. *Macromolecules* **2007**, *40* (2), 344−354.
(31) Sankar, U. K.; Tripathy, M. Dispersion, depletion, and bridging of athermal and attractive nanorods in polymer melt. *Macromolecules* **2015**, *48* (2), 432−442.
(32) Karatrantos, A.; Clarke, N.; Kröger, M. Modeling of polymer structure and conformations in polymer nanocomposites from atomistic to mesoscale: A review. *Polym. Rev.* **2016**, *56* (3), 385−428.
(33) Starr, F. W.; Schrøder, T. B.; Glotzer, S. C. Molecular dynamics simulation of a polymer melt with a nanoscopic particle. *Macromolecules* **2002**, *35* (11), 4481−4492.
(34) Jouault, N.; Dalmas, F.; Said, S.; Di Cola, E.; Schweins, R.; Jestin, J.; Boué, F. Direct measurement of polymer chain conformation in well-controlled model nanocomposites by combining SANS and SAXS. *Macromolecules* **2010**, *43* (23), 9881−9891.
(35) Crawford, M. K.; Smalley, R. J.; Cohen, G.; Hogan, B.; Wood, B.; Kumar, S. K.; Melnichenko, Y. B.; He, L.; Guise, W.; Hammouda, B. Chain conformation in polymer nanocomposites with uniformly dispersed nanoparticles. *Phys. Rev. Lett.* **2013**, *110* (19), 196001.
(36) Karatrantos, A.; Clarke, N.; Composto, R. J.; Winey, K. I. Polymer conformations in polymer nanocomposites containing spherical nanoparticles. *Soft Matter* **2015**, *11* (2), 382−388.
(37) Rizk, M.; Krutyeva, M.; Lühmann, N.; Allgaier, J.; Radulescu, A.; Pyckhout-Hintzen, W.; Wischnewski, A.; Richter, D. A Small-Angle Neutron Scattering Study of a Soft Model Nanofiller in an Athermal Melt. *Macromolecules* **2017**, *50* (12), 4733−4741.
(38) Robbes, A.-S.; Cousin, F.; Meneau, F.; Jestin, J. Melt chain conformation in nanoparticles/polymer nanocomposites elucidated

by the SANS extrapolation method: evidence of the filler contribution. *Macromolecules* **2018**, *51* (6), 2216−2226.
(39) Nakatani, A. I.; Chen, W.; Schmidt, R. G.; Gordon, G. V.; Han, C. C. Chain dimensions in polysilicate-filled poly(dimethyl siloxane). *Polymer* **2001**, *42* (8), 3713−3722.
(40) Mackay, M. E.; Tuteja, A.; Duxbury, P. M.; Hawker, C. J.; Van Horn, B.; Guan, Z.; Chen, G.; Krishnan, R. General strategies for nanoparticle dispersion. *Science* **2006**, *311* (5768), 1740−1743.
(41) Tuteja, A.; Duxbury, P. M.; Mackay, M. E. Polymer chain swelling induced by dispersed nanoparticles. *Phys. Rev. Lett.* **2008**, *100* (7), 21−24.
(42) Frischknecht, A. L.; McGarrity, E. S.; Mackay, M. E. Expanded chain dimensions in polymer melts with nanoparticle fillers. *J. Chem. Phys.* **2010**, *132* (20), 204901.
(43) Sorichetti, V.; Hugouvieux, V.; Kob, W. Structure and dynamics of a polymer−nanoparticle composite: Effect of nanoparticle size and volume fraction. *Macromolecules* **2018**, *51* (14), 5375−5391.
(44) Jouault, N.; Crawford, M. K.; Chi, C.; Smalley, R. J.; Wood, B.; Jestin, J.; Melnichenko, Y. B.; He, L.; Guise, W. E.; Kumar, S. K. Polymer Chain Behavior in Polymer Nanocomposites with Attractive Interactions. *ACS Macro Lett.* **2016**, *5* (4), 523−527.
(45) Jouault, N.; Kumar, S. K.; Smalley, R. J.; Chi, C.; Moneta, R.; Wood, B.; Salerno, H.; Melnichenko, Y. B.; He, L.; Guise, W. E.; Hammouda, B.; Crawford, M. K. Do Very Small POSS Nanoparticles Perturb s-PMMA Chain Conformations? *Macromolecules* **2018**, *51* (14), 5278−5293.
(46) Vacatello, M. Monte Carlo simulations of polymer melts filled with solid nanoparticles. *Macromolecules* **2001**, *34* (6), 1946−1952.
(47) Vacatello, M. Chain dimensions in filled polymers: An intriguing problem. *Macromolecules* **2002**, *35* (21), 8191−8193.
(48) Li, C.-Y.; Qian, C.-J.; Yang, Q.-H.; Luo, M.-B. Study on the polymer diffusion in a media with periodically distributed nano-sized fillers. *J. Chem. Phys.* **2014**, *140* (10), 104902.
(49) Li, C.-Y.; Luo, M.-B.; Huang, J.-H.; Li, H. Equilibrium and dynamical properties of polymer chains in random medium filled with randomly distributed nano-sized fillers. *Phys. Chem. Chem. Phys.* **2015**, *17* (47), 31877−31886.
(50) Huang, X.-W.; Peng, Y.; Huang, J.-H. Universal behaviors of polymer conformations in crowded environment. *Colloid Polym. Sci.* **2018**, *296* (4), 689−696.
(51) Erguney, F. M.; Lin, H.; Mattice, W. L. Dimensions of matrix chains in polymers filled with energetically neutral nanoparticles. *Polymer* **2006**, *47* (10), 3689−3695.
(52) Li, C.-Y.; Huang, J.-H.; Li, H.; Luo, M.-B. Study on the interfacial properties of polymers around a nanoparticle. *RSC Adv.* **2020**, *10* (47), 28075−28082.
(53) Tung, W.-S.; Bird, V.; Composto, R. J.; Clarke, N.; Winey, K. I. Polymer chain conformations in CNT/PS nanocomposites from small angle neutron scattering. *Macromolecules* **2013**, *46* (13), 5345−5354.
(54) Kim, S. Y.; Schweizer, K. S.; Zukoski, C. F. Multiscale structure, interfacial cohesion, adsorbed layers, and thermodynamics in dense polymer-nanoparticle mixtures. *Phys. Rev. Lett.* **2011**, *107* (22), 225504.
(55) Jouault, N.; Moll, J. F.; Meng, D.; Windsor, K.; Ramcharan, S.; Kearney, C.; Kumar, S. K. Bound polymer layer in nanocomposites. *ACS Macro Lett.* **2013**, *2* (5), 371−374.
(56) Li, Y.; Kröger, M.; Liu, W. K. Dynamic structure of unentangled polymer chains in the vicinity of non-attractive nanoparticles. *Soft Matter* **2014**, *10* (11), 1723−1737.
(57) Griffin, P. J.; Bocharova, V.; Middleton, L. R.; Composto, R. J.; Clarke, N.; Schweizer, K. S.; Winey, K. I. Influence of the Bound Polymer Layer on Nanoparticle Diffusion in Polymer Melts. *ACS Macro Lett.* **2016**, *5* (10), 1141−1145.
(58) Huang, J.-H.; Sun, D.-D.; Lu, R.-X.; Zhang, H.; Khan, R. A. A. Simulation on diffusivity and statistical size of polymer chains in polymer nanocomposites. *Phys. Chem. Chem. Phys.* **2020**, *22* (38), 21919−21927.
(59) Nie, Z.; Fava, D.; Rubinstein, M.; Kumacheva, E. Supramolecular" assembly of gold nanorods end-terminated with polymer "pom-poms": effect of pom-pom structure on the association modes. *J. Am. Chem. Soc.* **2008**, *130* (11), 3683−3689.
(60) Umadevi, S.; Feng, X.; Hegmann, T. Large Area Self-Assembly of Nematic Liquid-Crystal-Functionalized Gold Nanorods. *Adv. Funct. Mater.* **2013**, *23* (11), 1393−1403.
(61) Malvankar, N. S.; Vargas, M.; Nevin, K.; Tremblay, P.-L.; Evans-Lutterodt, K.; Nykypanchuk, D.; Martz, E.; Tuominen, M. T.; Lovley, D. R. Structural basis for metallic-like conductivity in microbial nanowires. *mBio* **2015**, *6* (2), e00084.
(62) Grest, G. S.; Kremer, K. Molecular dynamics simulation for polymers in the presence of a heat bath. *Phys. Rev. A: At., Mol., Opt. Phys.* **1986**, *33* (5), 3628.
(63) Cotter, M. A.; Martire, D. E. Statistical mechanics of rodlike particles. II. A Scaled Particle investigation of the aligned→ isotropic transition in a fluid of rigid spherocylinders. *J. Chem. Phys.* **1970**, *52* (4), 1909−1919.
(64) Yatsenko, G.; Schweizer, K. S. Ideal vitrification, barrier hopping, and jamming in fluids of modestly anisotropic hard objects. *Phys. Rev. E* **2007**, *76* (4), 041506.
(65) Ghobadi, A. F.; Jayaraman, A. Effect of backbone chemistry on hybridization thermodynamics of oligonucleic acids: a coarse-grained molecular dynamics simulation study. *Soft Matter* **2016**, *12* (8), 2276−87.
(66) Ghobadi, A. F.; Jayaraman, A. Effects of Polymer Conjugation on Hybridization Thermodynamics of Oligonucleic Acids. *J. Phys. Chem. B* **2016**, *120* (36), 9788−99.
(67) Condon, J. E.; Jayaraman, A. Effect of oligonucleic acid (ONA) backbone features on assembly of ONA-star polymer conjugates: a coarse-grained molecular simulation study. *Soft Matter* **2017**, *13* (38), 6770−6783.
(68) Condon, J. E.; Jayaraman, A. Development of a Coarse-Grained Model of Collagen-Like Peptide (CLP) for Studies of CLP Triple Helix Melting. *J. Phys. Chem. B* **2018**, *122* (6), 1929−1939.
(69) Beltran-Villegas, D. J.; Intriago, D.; Kim, K. H. C.; Behabtu, N.; Londono, J. D.; Jayaraman, A. Coarse-grained molecular dynamics simulations of α-1,3-glucan. *Soft Matter* **2019**, *15* (23), 4669−4681.
(70) Kulshreshtha, A.; Modica, K. J.; Jayaraman, A. Impact of Hydrogen Bonding Interactions on Graft-Matrix Wetting and Structure in Polymer Nanocomposites. *Macromolecules* **2019**, *52* (7), 2725−2735.
(71) Prhashanna, A.; Taylor, P. A.; Qin, J.; Kiick, K. L.; Jayaraman, A. Effect of Peptide Sequence on the LCST-Like Transition of Elastin-Like Peptides and Elastin-Like Peptide-Collagen-Like Peptide Conjugates: Simulations and Experiments. *Biomacromolecules* **2019**, *20* (3), 1178−1189.
(72) Prhashanna, A.; Jayaraman, A. Melting thermodynamics of oligonucleic acids conjugated with relatively solvophobic linear polymers: A coarse-grained molecular simulation study. *J. Polym. Sci., Part B: Polym. Phys.* **2019**, *57* (18), 1196−1208.
(73) Wu, Z.; Beltran-Villegas, D. J.; Jayaraman, A. Development of a New Coarse-Grained Model to Simulate Assembly of Cellulose Chains Due to Hydrogen Bonding. *J. Chem. Theory Comput.* **2020**, *16* (7), 4599−4614.
(74) Taylor, P. A.; Huang, H.; Kiick, K. L.; Jayaraman, A. Placement of tyrosine residues as a design element for tuning the phase transition of elastin-peptide-containing conjugates: experiments and simulations. *Molecular Systems Design & Engineering* **2020**, *5* (7), 1239−1254.
(75) Jayaraman, A. 100th Anniversary of Macromolecular Science Viewpoint: Modeling and Simulation of Macromolecules with Hydrogen Bonds: Challenges, Successes, and Opportunities. *ACS Macro Lett.* **2020**, *9* (5), 656−665.
(76) Heo, K.; Miesch, C.; Emrick, T.; Hayward, R. C. Thermally reversible aggregation of Gold nanoparticles in polymer nanocomposites through hydrogen bonding. *Nano Lett.* **2013**, *13* (11), 5297−302.
(77) Leung, F. C. M.; Leung, S. Y. L.; Chung, C. Y. S.; Yam, V. W. W. Metal-Metal and Interactions Directed End-to-End Assembly of Gold Nanorods. *J. Am. Chem. Soc.* **2016**, *138* (9), 2989−2992.

(78) Chan, Y.-T.; Li, S.; Moorefield, C. N.; Wang, P.; Shreiner, C. D.; Newkome, G. R. Self-Assembly, Disassembly, and Reassembly of Gold Nanorods Mediated by Bis(terpyridine)−Metal Connectivity. *Chem. - Eur. J.* **2010**, *16* (14), 4164−4168.
(79) Miller, T. F.; Eleftheriou, M.; Pattnaik, P.; Ndirango, A.; Newns, D.; Martyna, G. Symplectic quaternion scheme for biophysical molecular dynamics. *J. Chem. Phys.* **2002**, *116* (20), 8649−8659.
(80) Jones, J. E.; Chapman, S. On the determination of molecular fields. —II. From the equation of state of a gas. *Proc. R. Soc. London A* **1924**, *106* (738), 463−477.
(81) Weeks, J. D.; Chandler, D.; Andersen, H. C. Role of Repulsive Forces in Determining the Equilibrium Structure of Simple Liquids. *J. Chem. Phys.* **1971**, *54* (12), 5237−5247.
(82) Plimpton, S. Fast parallel algorithms for short-range molecular-dynamics. *J. Comput. Phys.* **1995**, *117* (1), 1−19.
(83) Cormen, T. H.; Leiserson, C. E.; Rivest, R. L.; Stein, C. *Introduction to algorithms*; MIT press: 2009.
(84) Humphrey, W.; Dalke, A.; Schulten, K. VMD: visual molecular dynamics. *J. Mol. Graphics* **1996**, *14* (1), 33−38.
(85) Mao, Y.; Cates, M. E.; Lekkerkerker, H. N. W. Depletion force in colloidal systems. *Phys. A* **1995**, *222* (1), 10−24.

https://dx.doi.org/10.1021/acs.jpcb.1c00097
J. Phys. Chem. B 2021, 125, 2435−2449